A THEORETICAL STUDY OF FLUID FORCES ON A CENTRIFUGAL IMPELLER ROTATING AND WHIRLING IN A VANED DIFFUSER

Yoshinobu Tsujimoto
Osaka University
Toyonaka, Osaka, 560, Japan

Allan J. Acosta
California Institute of Technology
Pasadena, California 91125, U.S.A.

Yoshiki Yoshida
Mitsubishi Heavy Industry
Takasago, Hyogo, 676, Japan

The fluid forces on a centrifugal impeller rotating and whirling in a vaned diffuser are analysed on the assumption that the number of impeller and diffuser vanes is so large that the flows are perfectly guided by the vanes. The flow is taken to be two dimensional, inviscid, and incompressible, but the effects of impeller and diffuser losses are taken into account.

It is shown that the interaction with the vaned diffuser may cause destabilizing fluid forces for whirling motion even at design flow rate. Discussions are made to elucidate the physical mechanisms that produce the destabilizing fluid forces. From these discussions, it is found that the whirling forces are closely related to the steady head-capacity characteristics of the impeller. This physical understanding of the whirling forces can be applied also to the cases with volute casings.

At partial capacities, it is shown that the impeller forces change greatly when the flow rate and whirl velocity are near to the impeller or vaned diffuser attributed rotating stall onset capacity, and the stall propagation velocity, respectively. In such cases the impeller forces may become destabilizing for impeller whirl.

INTRODUCTION

It has been made clear by pioneering experiments by Ohashi et al. (ref. 1) and Acosta et al. (refs. 2 and 3) that the fluid forces on centrifugal impellers may become destabilizing for whirling motion under certain conditions. Even if the impeller forces are stabilizing, it is important to estimate the forces since there are many cases in which the whirling instability is caused by bearing or seal forces.

So far the following examples have been reported in which the impeller forces become destabilizing for whirl. Ohashi et al. (ref. 1) have measured whirling forces on two-dimensional impellers in vaned or vaneless diffusers to capture the basic nature of the forces and to compare with their two-dimensional potential flow analyses (refs. 4 and 5). In this, it was found that the forces are basically stabilizing but become destabilizing for whirling with small positive whirl velocity

ratios at partial capacity. Recently new testing equipment was developed (ref. 6), and preliminary results on a three-dimensional boiler feed pump impeller model whirling in a vaned diffuser were reported. The impeller forces become very large compared with the 2D cases, but they are stabilizing both at design and shut off capacities.

Acosta et al. focused on the interaction with the volute casing and have shown that the forces on impellers whirling in a volute may become destabilizing even at design capacity (refs. 2, 3 and 7). A two-dimensional unsteady flow analysis (ref. 8) was carried out assuming that the impeller has an infinite number of vanes, and it was found that it can simulate the experimental results fairly well.

Bolleter and Wyss (ref. 9) used a "rocking arm" test apparatus to measure force matrices of a boiler feed pump impeller with outlet guide vanes. Whirling forces were synthesized on the assumption of the linearity of the disturbance, and it was shown that the forces are destabilizing for small positive whirl even at design capacity.

Two of the present authors have made an analysis (ref. 10) of impeller forces on a two-dimensional impeller whirling in a vaneless diffuser. There, it was shown that the whirling forces are basically stabilizing, as shown by Ohashi et al. (ref. 1), but they may become destabilizing if the flow rate and the whirling velocity are near the onset flow rate and the stall propagation velocity of rotating stalls due to the impeller or the vaneless diffuser.

The present study treats the cases when a impeller whirls in a vaned diffuser on the assumption of a two-dimensional inviscid incompressible flow. The number of impeller and/or diffuser vanes is taken to be infinite, and the total pressure losses in the impeller and the diffuser are taken into account. It is assumed that the outlet of the diffuser is open to a space of constant pressure. The problem is linearized on the assumption that the eccentricity and hence the unsteady components are sufficiently small.

FLOW ANALYSIS

We consider the case when, as shown in Fig. 1, a logarithmic centrifugal impeller with a vane angle β and inner and outer radii r_1 and r_2 rotates with an angular velocity Ω and whirls with an eccentricity ε and an angular velocity ω, in a logarithmic vaned diffuser with a vane angle α, inner and outer radii r_3 and r_4. We take a stationary frame $z' = x' + iy' = r'e^{i\theta'}$ with its origin at the center of the diffuser, and a moving frame $z = x + iy = re^{i\theta}$ with its origin at the center of the impeller translating with its axes parallel to the stationary frame. We put $'$ on the velocities relative to the z' frame, and the velocities without $'$ represent the velocities relative to the z frame. The total velocity and the steady and unsteady components are represented by v, V, and v_d, respectively. For unsteady components, we use a complex representation with respect to an imaginary unit j such as $v_{rpd} = \tilde{v}_{rp} \exp\{j(\omega t - \theta)\}$ where the suffix r means radial component and $p = 1, 2, 3, 4$ means the values at $r = r_1$, r_2, r_3, and r_4. We consider that the real part carries the physical meaning.

Relations governing unsteady components

The results of the relations and expressions obtained for the vaneless diffuser case (ref. 10) could also be used here.

Velocity at the impeller inlet: The velocity disturbance is composed of that due to relative dislocation of a source Q at the origin of the z' frame and an unknown potential disturbance

$$\tilde{v}_{r1} = -\varepsilon Q/(2\pi r_1^2) + v_{r1}^* \tag{1}$$

$$\tilde{v}_{\theta 1} = -\varepsilon Q j/(2\pi r_1^2) - j v_{r1}^* \tag{2}$$

where v_{r1}^* is an unknown complex constant.

Velocities at the impeller outlet and the diffuser inlet ($p = 2, 3$): The steady velocity in the vaneless part ($r_2 < r < r_3$) is given by $(V_r, V_\theta) = (Q/2\pi r, \Gamma/2\pi r)$ where $\Gamma = 2\pi r_2[r_2\Omega - Q/(2\pi r_2)\cot\beta]$ is the impeller circulation. We assume a vorticity ζ shed from the impeller is transported at this steady velocity. Then the unsteady velocities can be given as a sum of the velocity induced by the vorticity field of magnitude ζ_2 and a potential flow disturbance of strength $\tilde{A}$.

$$\tilde{v}_{rp} = Z_{rp}\zeta_2 + A_{rp}\tilde{A} \tag{3}$$

$$\tilde{v}_{\theta p} = Z_{\theta p}\zeta_2 + A_{\theta p}\tilde{A} \tag{4}$$

where

$$Z_{rp} = (R_R - jR_I)_{rp} - (r_2/r_p)^2 e^{-2j\beta} (R_R - jR_I)_{r2}$$

$$Z_{\theta p} = (\Theta_R - j\Theta_I)_{rp} - j(r_2/r_p)^2 e^{-2j\beta} (R_R - jR_I)_{r2}$$

$$A_{rp} = 1 - (r_2/r_p)^2 e^{-2j\beta}, \quad A_{\theta p} = -j\{1 + (r_2/r_p)^2 e^{-2j\beta}\}$$

$$R_R - jR_I = -j(S + T), \quad \Theta_R - j\Theta_I = S - T$$

$$S(r) = (1/2)\int_{r_2}^{r} \lambda(r_0, 0)(r_0/r)^2 \, dr_0$$

$$T(r) = (1/2)\int_{r}^{r_3} \lambda(r_0, 0) \, dr_0$$

$$\lambda(r,\theta) = \exp([-j\{\pi\omega(r^2 - r_2^2)/Q + \theta - (\Gamma/Q)\log(r/r_2)\}])$$

The expressions (3) and (4) are so determined that the flow tangency condition at the impeller outlet $\tilde{v}_{\theta 2} = -\tilde{v}_{r2}\cot\beta$ is satisfied.

Continuity of mass flow between impeller inlet and outlet: Defining $\phi \equiv \theta_1 - \theta_2 = \cot\beta \log(r_2/r_1)$ as shown in Fig. 1, we obtain the following continuity relation between $r = r_1$ and r_2.

$$r_1\tilde{v}_{r1} = r_2\tilde{v}_{r2}e^{j\phi} \tag{5}$$

Strength of shed vorticity: We obtain the following expression by integrating the momentum equation from inlet to outlet of the impeller and using the θ component of Euler's equation at the impeller outlet.

$$r_2 V_{r2}\,\zeta_2 = J\tilde{v}_{r2} + D \tag{6}$$

where

$$J = (\omega - \Omega)\{r_2(1 + j\cot\beta) + M\} - jL_1$$

$$D = \varepsilon Q e^{-j\phi}\{2r_1(\omega - \Omega) - L_2\}/(2\pi r_1^2)$$

and $M \equiv \int_{r_3}^{r_2} r_2/(r\sin\beta)ds = r_2(\sin\beta)^{-2}\log(r_2/r_1)$ is the effective length of the flow channel of the impeller, L_1 and L_2 are parameters representing the effects of total pressure loss in the impeller. These are given as follows. We assume that the loss can be given as a sum of incidence and hydraulic losses:

$$\Delta p_t/\rho = \{\zeta_s(1/t_a - 1/t_{ad})^2 + \zeta^*\}v_{r1}^2/2 \equiv Z(t_a)v_{r1}^2/2 \tag{7}$$

where t_a is the tangent of the mean flow inlet angle $\bar{\beta}_1$, and $t_{ad} = \tan\beta$. The hydraulic and incidence loss coefficients ζ^* and ζ_s are evaluated from

$$\zeta^* = 2(1 - \eta_h)(r_1/r_2)^2(1 - \phi_d\cot\beta)/\phi_d^2$$

$$\zeta_s = 0.3 + 0.6\beta°/90°$$

using the shock free flow coefficient ϕ_d and the impeller efficiency η_h at ϕ_d. For simplicity, we neglect the delay of loss and evaluate the loss from quasi-steady application of equation (7). After linearization on the assumption that the disturbance is small, we obtain the following expressions for L_1 and L_2:

$$L_1 = V_{r1}(r_2/r_1)\{Z + (1/2)\tan\bar{\beta}_1(1 - j\tan\bar{\beta}_1)Z'\}$$

$$L_2 = V_{r1}\,Z'\tan^2\bar{\beta}_1$$

The condition at diffuser outlet

We assume that the outlet of the diffuser is connected to a space of constant pressure. From this condition, we derive a relation that should be satisfied at the diffuser inlet. Taking the total pressure loss Δp_{td} in the diffuser into account, we can express the unsteady Bernoulli's equation as follows.

$$p_3/\rho = p_4/\rho + 1/2(v_4'^2 - v_3'^2) + \int_{r_3}^{r_4} \partial v_s'/\partial t \cdot ds + \Delta p_{td}/\rho \tag{8}$$

We evaluate Δp_{td} by equation (7) after replacements of $Z(t_a)$ with $Z_d(\tan\bar{\alpha}_3)$ and v_{r1} with v'_{r3}. After the linearization of equation (8) with respect to the unsteady component and the differentiation with θ', we obtain

$$1/\rho \cdot \partial p_3/\partial\theta_3' = -j[(E_d + L_{1d})\tilde{v}_{r3}' - (\Gamma/2\pi r_3 + L_{2d}/2)\tilde{v}_{\theta 3}'] \tag{9}$$

where

$$E_d = V_{r4}(r_3/r_4)(1 + \cot^2\alpha) - V_{r3} + j\omega M_d$$

M_d = effective length of diffuser flow channel

$= r_3(\sin\alpha)^{-2}\log(r_3/r_4)$

$L_{1d} = Z_d V_{r3} + (1/2)V_{r3}Z_d' \tan\bar{\alpha}_3$

$L_{2d} = V_{r3}Z_d' \tan^2\bar{\alpha}_3$

and the relation $\partial p_4/\partial\theta_3' = 0$ has been used. $\bar{\alpha}_3 = \tan^{-1}(Q/\Gamma)$ is the mean flow angle at the diffuser inlet.

The unsteady component of the absolute velocity at the diffuser inlet is given as a sum of the unsteady component in the moving frame, a component due to the dislocation of the steady flow field (V_r, V_θ), and the whirling velocity:

$$\tilde{v}_{r3}' = \tilde{v}_{r3} + \varepsilon(Q - j\Gamma)/2\pi r_3^2) + \varepsilon\omega j$$

$$\tilde{v}_{\theta 3}' = \tilde{v}_{\theta 3} + \varepsilon(\Gamma + jQ)/2\pi r_3^2) + \varepsilon\omega \qquad (10)$$

Putting equations (9) and (10) in the θ' component of a linearized Euler's equation, we finally obtain the following equation representing the diffuser outlet condition.

$$P_\zeta \bar{\zeta}_2 + P_A\tilde{A} = G \qquad (11)$$

where

$$P_\zeta = (j\omega + V_{r3}/r_3 + jL_{2d}/2r_3)Z_{\theta 3} - j(E_d + L_{1d})Z_{r3}/r_3 + V_{r3}Z_a$$

$$P_A = (j\omega + V_{r3}/r_3 + jL_{2d}/2r_3)A_{\theta 3} - j(E_d + L_{1d})A_{r3}/r_3 - jZ_bV_{r3}$$

$$G = -\varepsilon(j\omega + V_{r3}/r_3 + jL_{2d}/2r_3)(\omega + V_{\theta 3}/r_3 + jV_{r3}/r_3)$$
$$+ \varepsilon j(E_d + L_{1d})(V_{r3}/r_3 + j\omega - jV_{\theta 3}/r_3)/r_3 + 2\varepsilon V_{r3}(V_{\theta 3} + jV_{r3})/r_3^2$$

$$Z_a = \lambda(r_3, 0) - 2S(r_3)/r_3 + 2j(r_2^2/r_3^3)e^{-2j\beta}\,(R_R - jR_1)_{r2}$$

$$Z_b = -2(r_2^2/r_3^3)e^{-2j\beta}$$

Determination of flow and impeller forces

From equations (1) to (6) and (11), we obtain

$$\tilde{A} = \{G(r_2V_{r2} - JZ_{r2}) - P_\zeta D\}/\{P_\zeta JA_{r2} + P_A(r_2V_{r2} - JZ_{r2})\} \qquad (12)$$

Other unknowns are determined by the successive use of equations (1) to (6) and (11). Each term of the numerator of the above equation has a factor ε. By considering the case with $\varepsilon = 0$, we find that the rotating stall onset conditions under the interaction of impeller and diffuser are obtained by setting the denominator of equation (12) to be zero.

The impeller forces are determined from the balance of momentum. If we separate the impeller forces into components normal to (n) and tangential to (t; positive counter clockwise) the whirling orbit, each component stays constant. The

impeller forces (F_n, F_t) normalized with $\rho\pi(r_2\Omega)^2\varepsilon$ are given by summing up the following components. ($\phi \equiv Q/2\pi r_2{}^2\Omega$ is a flow coefficient.)

Force due to inlet pressure

$$(F_n + jF_t)_{p1} = (r_1/r_2)[(\omega r_1/\Omega r_2)\{-2j(r_2/r_1)^2\phi + \omega/\Omega\} - \tilde{v}_{r2}/(\varepsilon\Omega)e^{j\phi}\{j\omega/\Omega + \phi(r_2/r_1)^2\}] \tag{13.1}$$

Force due to inlet momentum

$$(F_n + jF_t)_{m1} = \phi[2\phi(r_2/r_1)^2 + 2j\omega/\Omega + 3e^{j\phi}\,\tilde{v}_{r2}(r_2/r_1)/\varepsilon\Omega] \tag{13.2}$$

Force due to outlet pressure

$$\begin{aligned}(F_n + jF_t)_{p2} = {} & -(\omega/\Omega)^2 - je^{-j\phi}\,(L_2/r_2\Omega)\phi(r_2/r_1)^2 \\ & - 2j\phi(r_2/r_1)e^{-j\phi}(1 - \omega/\Omega) \\ & - \{j(1 + M/r_2)(1 - \omega/\Omega) - \phi(1 + \cot^2\beta) \\ & - L_1/(r_2\Omega)\}\tilde{v}_{r2}/(\varepsilon\Omega)\end{aligned} \tag{13.3}$$

Force due to outlet momentum

$$(F_n + jF_t)_{m2} = -\{2\phi + j(1 - 2\phi\,\cot\beta\}\tilde{v}_{r2}/(\varepsilon\Omega) - 2j\phi(\omega/\Omega) \tag{13.4}$$

Force due to change of momentum of the fluid in the impeller

$$(F_n + jF_t)_m = -j(\omega/\Omega)\{1 - (r_1/r_2)e^{j\phi}\}\tilde{v}_{r2}/(\varepsilon\Omega) + (\omega/\Omega)^2\{1 - (r_1/r_2)^2\} \tag{13.5}$$

RESULTS AND DISCUSSIONS

We consider an impeller with $r_1/r_2 = 0.5$, $\beta = 30°$. The shock free flow coefficient for this impeller is $\phi_d \equiv v_{r2}/(r_2\Omega) = 0.1443$, which is looked upon as the "design" condition and is also shockless for diffusers with $\alpha = 11°$. The loss coefficients of the impeller were estimated from the equations shown in the last section assuming $\eta_h = 0.9$. The hydraulic loss coefficient for the diffuser was estimated from the expression of the coefficient after multiplying by $(r_2/r_1)^2$ and using $\eta_h = 0.9$. The diffuser incidence loss coefficient was obtained from the expression for the impeller after replacing β with α.

Impeller forces at design flow rate

Figure 2 shows the plots of F_n and F_t against the whirl velocity ratio ω/Ω. There, the diffuser inlet radius r_3 is changed keeping $(r_4 - r_3)/r_2$ to be 0.25. It has been known that if F_t is in the same direction as the whirl it is destabilizing, and vice versa. We find a destabilizing region for small positive whirl for $r_3/r_2 < 1.5$. This region diminishes with the increase of r_3/r_2. A similar destabilizing region is observed also for the cases with a volute. Discussions on this will be made shortly. F_n for $\omega/\Omega < 0$ increases with the decrease in r_3/r_2, which is considered to be caused by the increase of the apparent mass due to interaction with the vaned diffuser. If we increase r_3/r_2, F_n and F_t tend to the values for the case with a vaneless diffuser with outer radius $r_3/r_2 = 5.25$.

Figure 3 shows the effects of r_4/r_2. We see that F_n for $\omega/\Omega < 0$ increases with the increase in r_4/r_3, but F_t is not affected by r_4/r_3 systematically. Note that the destabilizing region exists even for the case with $r_4 = r_3$. On the other hand, if we change the vane angle α and r_4/r_3 keeping the effective length of the diffuser M_d to be constant, as shown in Figure 4, F_n does not change much but F_t for small positive to negative ω/Ω decreases with the increase in α. Now we can say that F_n for $\omega/\Omega < 0$ is mainly affected by M_d. F_t for $\omega/\Omega \lesssim 0.4$, and hence the existence of the destabilizing region, is largely dependent on the value of α.

In Figure 5 the impeller forces are separated into components corresponding to equations (13.1) to (13.5). We see that the component due to outlet pressure is dominant for $\omega/\Omega < 0.4$. Although not shown here, the contribution of outlet pressure is larger for the cases with smaller r_3/r_2. This is true also at partial capacities.

In all of the above calculations the effects of impeller and diffuser losses are taken into account. The above tendencies are not changed by neglecting the losses. After all, it is considered that the flow turning effect of the vaned diffuser is responsible for the existence of the destabilizing region.

Let us consider the physical mechanism with which the impeller forces become destabilizing. To simplify the problem we take the limits $r_3 \to r_2$ and $\alpha \to 0$. For such cases we can obtain a purely analytical solution without numerical integrations with respect to the shed vorticity. By letting $\alpha \to 0$ in the continuity equation $(v_4')^2 = (r_3/r_4)^2(v_{r3}')^2/\sin^2\alpha$, we find that a small increase in v_{r3}' in some part of the circumference results in a large increase in v_4' and hence in p_3 there, from equation (8). Then the outflow from the impeller to that part will be diminished; a diffuser with a small α has a smoothing effect on the circumferential flow rate distribution through the diffuser. By letting $\tilde{v}_{r3}' \to 0$ and $r_3 \to r_2$ in equation (10), we obtain

$$\tilde{v}_{r2} \to -\varepsilon(Q - j\Gamma)/(2\pi r_2^2) - \varepsilon\omega j$$

$$= \varepsilon\Omega[-\phi + \{(1 - \phi\cot\beta) - \omega/\Omega\}j] \tag{14}$$

This means that an outflow distribution $\tilde{v}_{r2}$ from the impeller is so determined as to cancel the radial absolute velocity disturbances due to the dislocation of the flow field of impeller circulation Γ and source Q and due to the whirling velocity. This equation can be obtained also by letting $\alpha \to 0$ in the analytical solution.

We estimate the impeller forces due to a pressure distribution which is obtained by assuming that the inertia on the fluid in the impeller due to $\tilde{v}_{r2}$ is balanced by the outlet pressure distribution. Then we have

$$(F_n + jF_t)_{p2} = -j(1 - \omega/\Omega)M\tilde{v}_{r2}/(r_2\varepsilon\Omega) \tag{15}$$

From the definition of complex representation, we find that the complex plot of $\tilde{v}_{r2}$ gives the azimuthal direction where the radial velocity becomes maximum and the amplitude of the radial velocity fluctuation, in a plane with its real axis in the direction of eccentricity (n) and the imaginary axis in the tangential (t) direction. Equation (14) shows that the radial velocity will become maximum in the direction $(n,t) = (-\phi, \psi \equiv 1 - \phi\cot\beta)$ for $\omega/\Omega = 0$ and the pressure in the direction $(-\psi, -\phi)$ where ϕ and ψ are flow and head coefficients. The resulting force is,

from equation (15), in the direction of (ψ, ϕ), i.e., outward and in the direction of rotation. Thus the impeller force is closely related to the steady impeller characteristics. F_n and F_t determined from equations (14) and (15) are given in the APPENDIX. Next is considered the effects of impeller loss. Near design flow rate, the loss becomes maximum in the direction of $\tilde{v}_{r2}$. There the outlet pressure is diminished and the resulting force can be expressed as $Z(r_2/r_1)^2 \phi \tilde{v}_{r2}/(\varepsilon\Omega)$, which is in the same direction as $\tilde{v}_{r2}$.

Figure 6 shows the above relations for $\alpha \to 0$ and $r_3/r_2 \to 1$ in which impeller and diffuser losses are neglected. This figure shows that equation (14) can estimate $\tilde{v}_{r2}$ fairly well for $\alpha = 1°$ and that the impeller force may be approximated by the outlet pressure force of equation (15) for $\omega/\Omega < 0$. Figure 7 shows an example for a more realistic case with $r_3/r_2 = 1.05$, $\alpha = 11°$ with the effects of losses taken into account. The absolute value of $\tilde{v}_{r2}$ is significantly smaller than that estimated from equation (14), which is mainly caused by the finiteness of α. We see that the impeller force may be estimated from the simple relations if we use the exact value of $\tilde{v}_{r2}$ in equation (15) and take into account the effect of loss discussed above. The real part of $\tilde{v}_{r2}$, and correspondingly F_t for $\omega/\Omega = 0$, approaches zero by increasing r_3/r_2 and hence the destabilizing region diminishes.

From the above discussions we may understand the mechanisms of the destabilizing impeller forces as follows. A vaned diffuser with a small vane angle α has the effect to smooth out the circumferential flow rate distribution through the diffuser. This effect brings about a circumferential flow distribution through the impeller to cancel out the absolute radial velocity disturbances at the diffuser inlet due to the dislocation of the flow field of impeller circulation Γ and source Q, and to the whirling velocity. Such a flow distribution through the impeller is established by a pressure distribution around the impeller, which balances with the inertia on the fluid in the impeller caused by the flow distribution. In cases of $\alpha \to 0$ and $r_3/r_2 \to 1$ the flow through the impeller for $\omega/\Omega = 0$ becomes maximum in the direction of $(n,t) = (-\phi,\psi)$ and the impeller force (F_n, F_t) due to the outlet pressure distribution caused by the flow distribution is positively proportional to (ψ, ϕ). This tendency is carried over to general cases of finite but small values of α and $r_3/r_2 \to 1$, resulting in a destabilizing region at small positive ω/Ω.

The tendencies that the outlet pressure force is more dominant for the cases of smaller r_3/r_2 and ω/Ω may be understood by considering that the above mechanism becomes more definitive for those cases. When the diffuser angle is not constant, the outlet angle will have a more important effect on the impeller forces. In cases with a volute, the radial velocity on the volute is strictly controlled by the volute surface. Hence the latter half of the above discussions can be applied also for the cases with a volute.

Impeller forces at partial capacity
(Cases with infinitesimally small impeller/diffuser gap)

We consider the cases with $r_3/r_2 \to 0$. As mentioned before, the solution becomes purely analytical for such cases. Figures 8 and 9 show the impeller forces at partial capacities with impeller and diffuser losses considered and neglected, respectively. For $\omega/\Omega < 0$, F_n increases and F_t decreases with the decrease in ϕ. This tendency can be understood from the discussions for $\alpha \to 0$ in the last section through the effect of ϕ on $\tilde{v}_{r2}$. The destabilizing region is enlarged by the decrease in ϕ. It is interesting to note here that the value of ω/Ω

for which $\mathrm{Imag}(\tilde{v}_{r2}) = 0$ increases with the decrease in ϕ. In Figure 7, the impeller forces for $\phi/\phi_d = 0.2$ change largely near $\omega/\Omega = 0.35$. This condition corresponds to the rotating stall onset flow rate and the stall propagation velocity which can be determined by putting the denominator of equation (12) to be zero. It can be shown that the onset flow rate thus determined equals the flow rate at which the difference between the diffuser outlet static pressure and the impeller inlet total pressure becomes unchanged by a change in flow rate. Those conditions agree with those obtained by Railly & Ekerol (ref. 11). The onset condition determined from equation (12) for this case is $(\phi/\phi_d, \omega/\Omega) = (0.21, 0.34)$. If we neglect the losses, as shown in Figure 8, we do not have the large change in the forces. For $\omega/\Omega < 0$, the losses have little effect on F_n but they have the effect to increase F_t near the design capacity and to decrease F_t at lower capacities. This is because the change in losses due to the change in incidence angle becomes significant at lower capacities. In Figures 8 and 9, we observe destabilizing regions in $\omega/\Omega < 0$ at very low capacities. This has not been observed experimentally, and it is questionable if the present model can be applied to such a small capacity.

Impeller forces at partial capacity (Cases with small impeller/diffuser gap)

At small capacities the impeller forces change largely with a small change in r_3/r_2 and the effect of rotating stall observed in Figure 7 for $r_3/r_2 = 1$ cannot be seen for $r_3/r_2 = 1.03$. Figure 10 shows the impeller forces for $r_3/r_2 = 1.10$. The impeller forces change greatly in the region $\omega/\Omega < 0$ at partial capacities. The denominator of equation (12) becomes zero for $(\phi/\phi_d, \omega/\Omega) = (0.288, -0.16)$. Unlike the cases with $r_3/r_2 = 1.0$ shown in Figures 8 and 9, the large change does not disappear by neglecting impeller and diffuser losses.

The vaned diffuser rotating stall onset condition can be obtained by a method similar to the present study under the assumptions that the pressure is constant at the outlet of the diffuser and that the flow upstream is irrotational. If we neglect the delay of loss, the onset flow rate coincides with that at which the difference of the inlet total pressure and the outlet static pressure is unaltered by the change in the flow rate under a constant inlet circumferential velocity. For the present case the diffuser rotating stall onset condition thus determined is $(\phi/\phi_d, \omega/\Omega) = (0.320, 0.0396)$. The impeller rotating stall onset condition for the present case determined under the condition of constant impeller outlet pressure is $(\phi/\phi_d, \omega/\Omega) = (0.349, 0.914)$ (ref. 10). Both of these conditions are far apart from the condition above mentioned.

As the flow rate gets smaller, the flow angle in the vaneless region becomes smaller and the time required for a fluid particle to pass through the region becomes larger. We consider a case when the shed vorticity decays proportionally to $\exp(-D_\alpha t)$, where D_α is a positive constant and t is the time passed after the vorticity is shed from the impeller. Such cases can be treated by simply multiplying $-D_\alpha \pi(r^2 - r_2^2)/Q$ by $\lambda(r,\theta)$ in equation (4). Figure 11 shows the results with $D_\alpha/\Omega = 2.0$. We do not have the large change in $\omega/\Omega < 0$ as seen in Fig. 10. This fact may show that the large change is caused by the interaction of the vorticity with the vaned diffuser. The denominator of equation (4) becomes zero for $(\phi/\phi_d, \omega/\Omega) = 0.40, 0.02)$, and the impeller forces change greatly near this condition. This condition is close to that of diffuser rotating stall onset. This large change in the impeller forces disappears if we neglect the diffuser loss. Hence, the large change for $D_\alpha/\Omega = 2.0$ is considered to be related to the diffuser rotating stall.

Impeller forces at partial capacity (Cases with large impeller/diffuser gap)

Figure 11 shows the results for $r_3/r_2 = 1.5$ and $D_\alpha/\Omega = 0.25$. The denominator of equation (12) becomes zero at $(\phi/\phi_d, \omega/\Omega) = (0.33, 0.02)$ and $(0.08, 0.98)$, near which the impeller forces change irregularly. The former and latter solutions disappear if we neglect the diffuser and impeller losses respectively. The diffuser and the impeller rotating stall onset conditions when they are alone are $(\phi/\phi_d, \omega/\Omega) = (0.328, 0.021)$ and $(0.349, 0.914)$, respectively, and these are close to the above conditions. Hence the irregular changes of the forces in Figure 12 are considered to be related to the diffuser and impeller rotating stalls. The change of the forces near the diffuser stall onset condition is smaller than that in Figure 11 for $r_3/r_2 = 1.1$. It decreases further by the increase in r_3/r_2. On the contrary, the impeller stall onset flow rate increases with the increase in r_3/r_2, and its effect on the impeller forces becomes more significant.

In any case the impeller forces change greatly near the diffuser and impeller rotating stall onset conditions and may become destabilizing for whirl. However, we should use a non-linear analysis for the exact determination of the impeller forces near rotating stall onset conditions, since rotating stalls are highly non-linear phenomena. In the present calculations with vaned diffusers, no phenomenon was observed which could be related to rotating stalls in the vaneless part of the diffuser.

CONCLUSIONS

Major findings of the present study may be summarized as follows.

(1) The fluid forces on an impeller whirling in a vaned diffuser may become destabilizing for whirling motion even at design capacity. Discussions are made to elucidate the cause of the destabilizing fluid forces, and it was shown that the destabilizing fluid forces are closely related to the steady head-capacity characteristics of the impeller.

(2) The destabilizing whirl velocity region is larger for a smaller diffuser vane angle, impeller/diffuser gap, and flow rate.

(3) For an infinitesimally small gap between impeller and diffuser, the effects of a rotating stall on the impeller forces are observed at partial capacity. These effects disappear with a small increase in the gap, but the effects of the interaction of shed vorticity with the vaned diffuser appear instead. If we take into account the decay of shed vorticity, effects of diffuser rotating stalls are observed.

(4) As we increase the gap further, the effects of the diffuser rotating stall become smaller. The impeller rotating stall onset flow rate increases and its effect on the impeller forces becomes more significant. In either case the impeller forces change greatly near the rotating stall onset conditions and may become destabilizing for impeller whirl.

(5) For small positive to negative whirl velocity ratio, the contribution of the impeller outlet pressure distribution has the most significant effect on the impeller forces. It increases as the impeller/diffuser gap is decreased.

APPENDIX
(Normal and tangential forces for $r_3/r_2 \to 1$ and $\alpha \to 0$, without loss)

From equation (14) and (15) we obtain

$$F_t = (M/r_2)(1 - \omega/\Omega)\phi$$

$$F_n = (M/r_2)(1 - \omega/\Omega)(\psi - \omega/\Omega)$$

where $\phi \equiv Q/2\pi r_2^2 \Omega$ is the flow coefficient and $\psi = 1 - \phi \cot \beta$ is the head coefficient (normalized by $\rho r_2^2\Omega^2$) of the impeller. M is the inertial length of the impeller flow channel, defined in the paragraph following equation (6).

These expressions show that F_t is linear with respect to ω/Ω and is proportional to the flow coefficient ϕ. F_n is a parabolic function of ω/Ω and dependent on the head coefficient ψ. These relations are illustrated in the following figure.

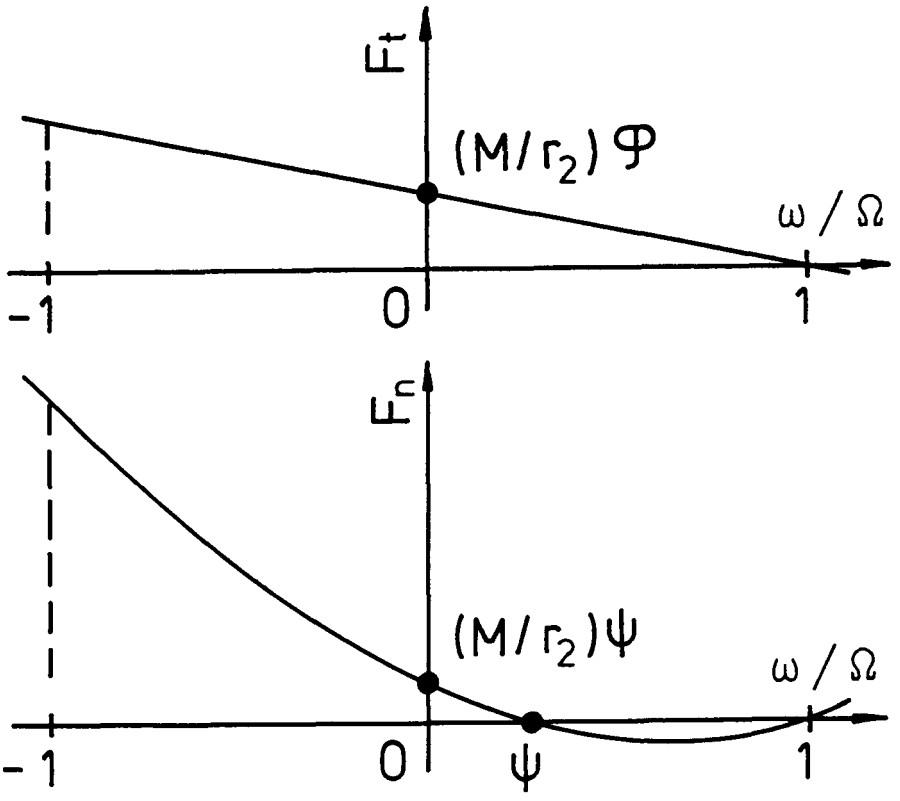

Illustration of F_t and F_n for the cases with $r_3/r_2 \to 1$ and $\alpha \to 0$, without losses.

The present authors would like to express their sincere gratitude to Professors H. Ohashi and C. Brennen for their helpful discussions. Acknowledgments are also made to Mr. S. Takatsugi for his assistance in numerical calculations.

REFERENCES

1. Ohashi, H. and Shoji, H., "Lateral Fluid Forces Acting on a Whirling Centrifugal Impeller," NASA CP-2335, May 1984, pp. 109-122.

2. Chamieh, D.S., Acosta, A.J., Brennen, C.E. and Caughey, T.K., "Experimental Measurements of Hydrodynamic Radial Forces and Stiffness Matrices for a Centrifugal Pump-Impeller," ASME Journal of Fluid Engineering, Vol. 107, No. 3, Sept. 1985, pp. 307-315.

3. Jery, B., Acosta, A.J., Brennen, C.E., Caughey, T.K. and Franz, R., "Experimental Measurements of Hydrodynamic Stiffness Matrices for a Centrifugal Pump-Impeller," NASA CP-2235, May 1984, pp. 137-160.

4. Shoji, H. and Ohashi, H., "Fluids Forces on Rotating Centrifugal Impeller With Whirling Motion," NASA CP-2133, May 1980, pp. 317-328.

5. Shoji, H. and Ohashi, H., "Theoretical Study of Fluid Forces on Whirling Centrifugal Impeller," (in Japanese), Trans. JSME, Vol. 50, no. 458, B. Oct. 1984, pp. 2518-2523.

6. Ohashi, H., Hatanaka, R. and Sakurai, A., "Fluid Force Testing Machine for Whirling Centrifugal Impeller," Proceedings of International Conference on Rotor Dynamics (IFToMM), Sept. 1986, Tokyo, pp. 643-648.

7. Arndt, N. and Franz, R., "Measurements of Hydrodynamic Forces on a Two-Dimensional Impeller and Modified Centrifugal Pump," Division of Engineering and Applied Science, California Institute of Technology, Rept. E249.4, 1986.

8. Tsujimoto, Y., Acosta, J. and Brennen, C., "Two-dimensional Unsteady Analysis of Fluid Forces on a Whirling Centrifugal Impeller in a Volute," NASA CP-2235, May 1984, pp. 161-171. Numerical results are included in "Theoretical Study of Fluid Forces on a Centrifugal Impeller Rotating and Whirling in a Volute," by the same authors, submitted to ASME Journal of Vibration, Acoustics, Stress and Reliability in Design.

9. Bolleter, U. and Wyss, A., "Measurement of Hydrodynamic Interaction Matrices of Boiler Feed Pump Impellers," ASME Paper 85-DET-148, 1985.

10. Tsujimoto, Y. and Acosta, A.J., "Theoretical Study of Impeller and/or Vaneless Diffuser Attributed Rotating Stalls and their Effects on Whirling Instability of a Centrifugal Impeller," Proceedings of IAHR Work Group on the Behavior of Hydraulic Machinery Under Steady Oscillatory Conditions, Sept. 1987, Lille, France.

11. Railly, J.W. and Ekerol, H., "Influence of a Closely Coupled Throttle on the Stalling Behavior of a Radial Compressor Stage," ASME Journal of Engineering for Gas Turbines and Power, Vol. 107, Apr. 1985, pp. 522-527.

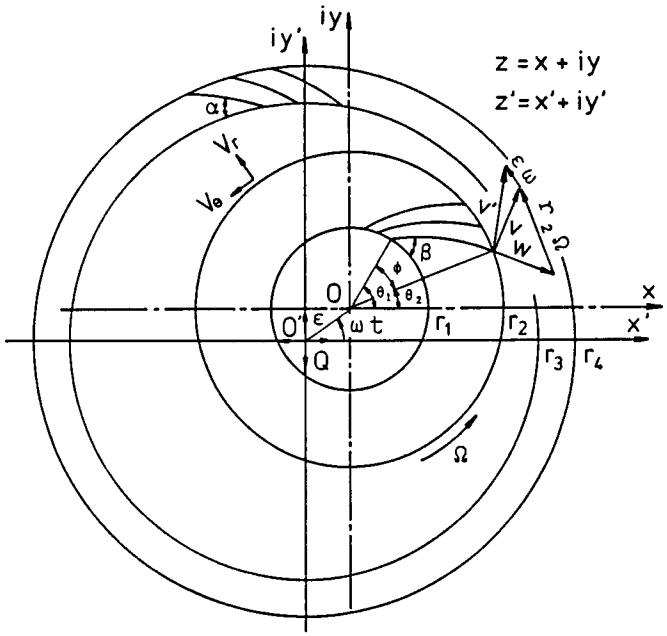

Fig.1 Impeller and vaned diffuser.

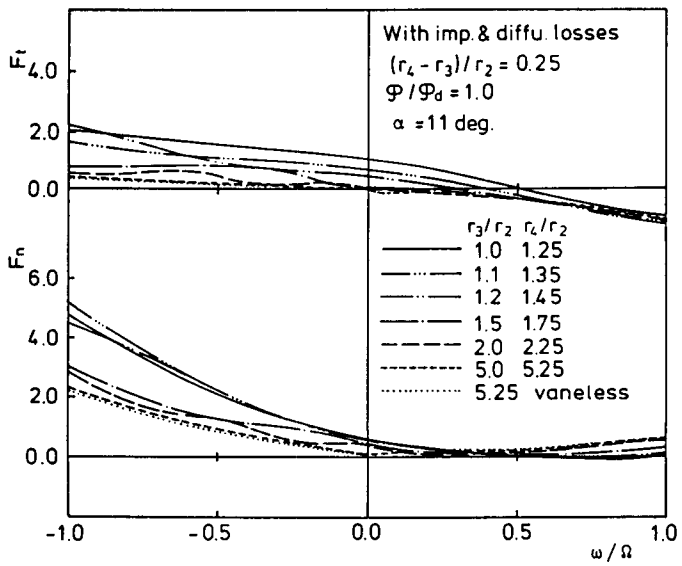

Fig.2 Effects of impeller/diffuser gap on whirling forces at design capacity.

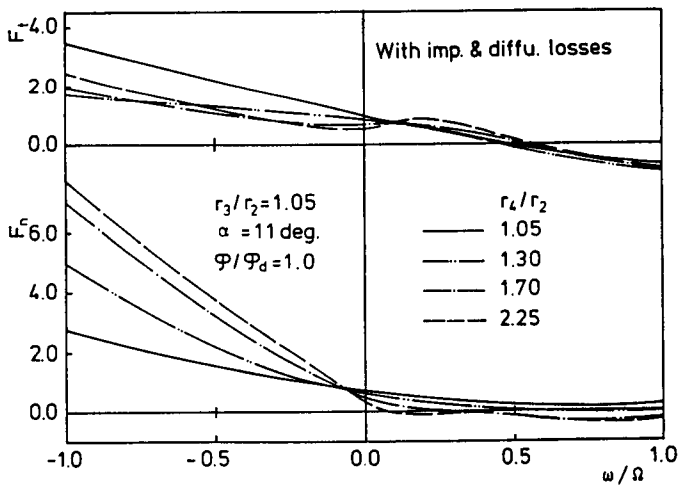

Fig.3 Effects of diffuser flow channel length on whirling forces at design capacity.

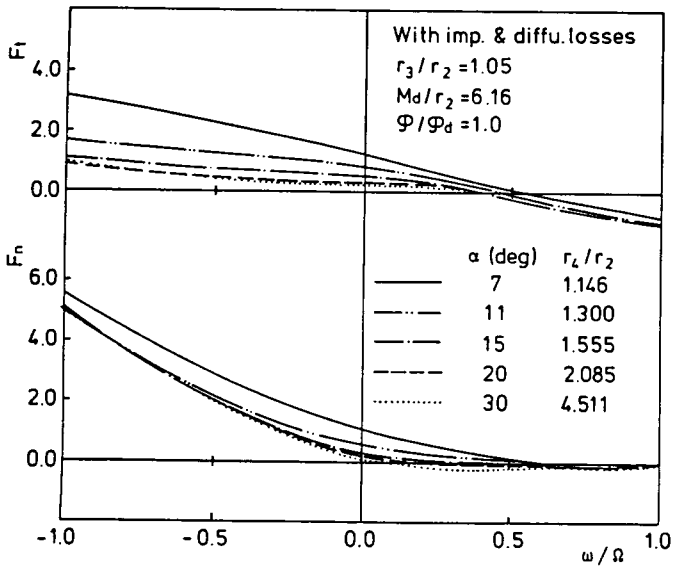

Fig.4 Effects of diffuser vane angle on whirling forces at design capacity. The effective length of diffuser flow channel is kept constant.

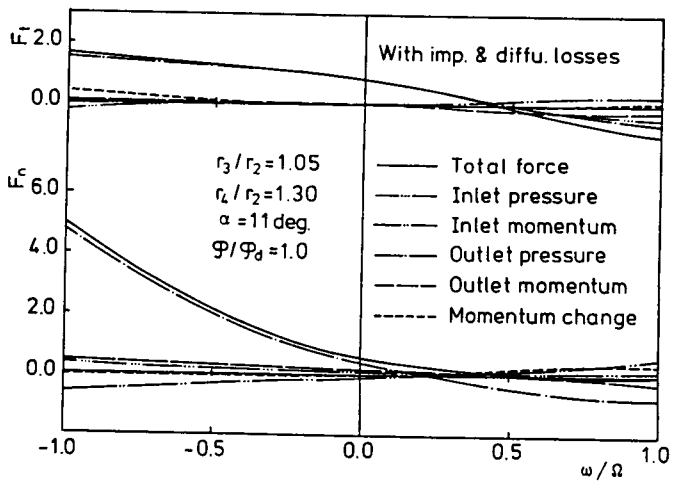

Fig.5 Division of whirling forces. Contribution of impeller outlet pressure distribution is dominant in a range of small positive to negative whirl velocity ratio.

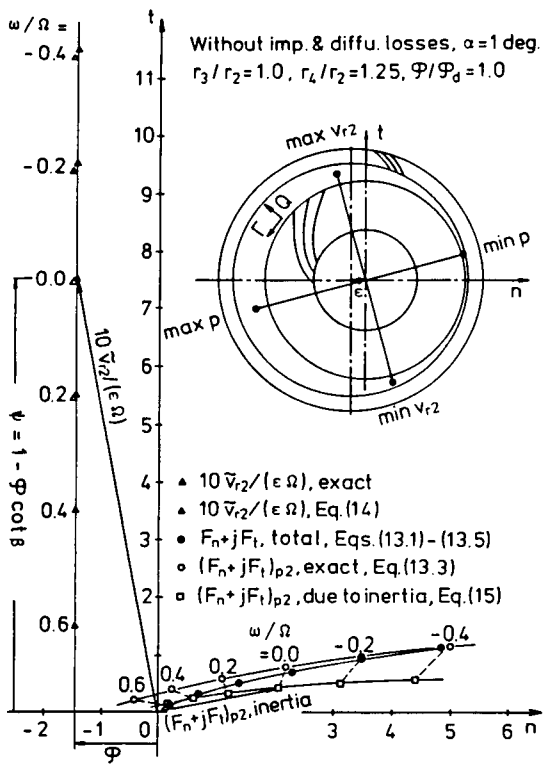

Fig.6 Illustration of the relations among impeller outlet flow distribution, pressure distribution and impeller forces, for an idealized case with $\alpha \to 0$ and $r_3 \to r_2$.

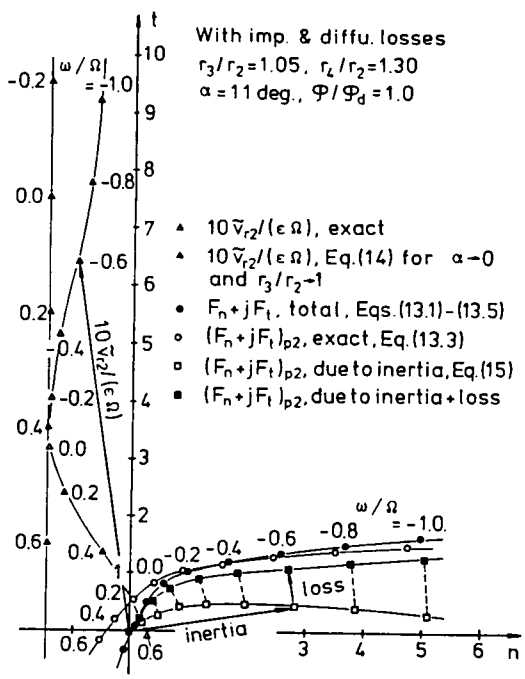

Fig.7 Illustration of the relations among impeller outlet flow distribution, pressure distribution and impeller forces, for a realistic case.

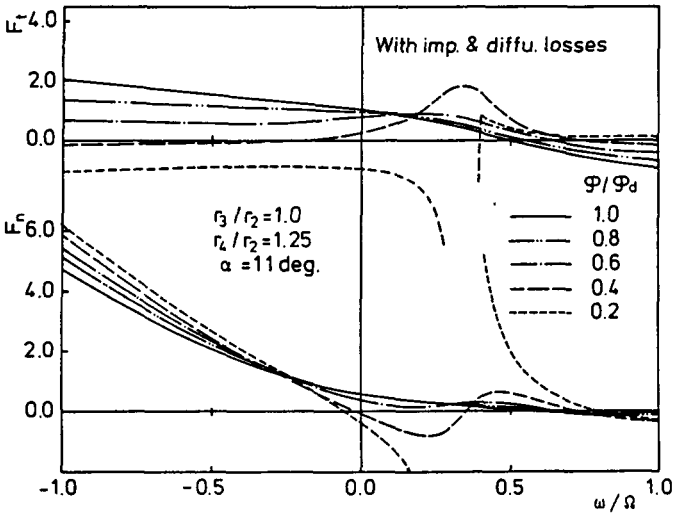

Fig.8 Impeller forces at partial capacities, for the case with infinitesimally small impeller/diffuser gap, with the effects of impeller and diffuser losses taken into account. Effects of a rotating stall are observed.

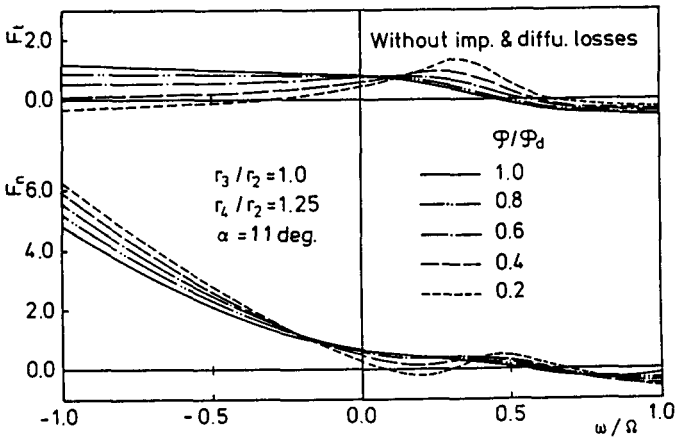

Fig.9 Impeller forces at partial capacities, for the case with infinitesimally small impeller/diffuser gap. The impeller and diffuser losses are not considered. We do not observe the effects of rotating stall.

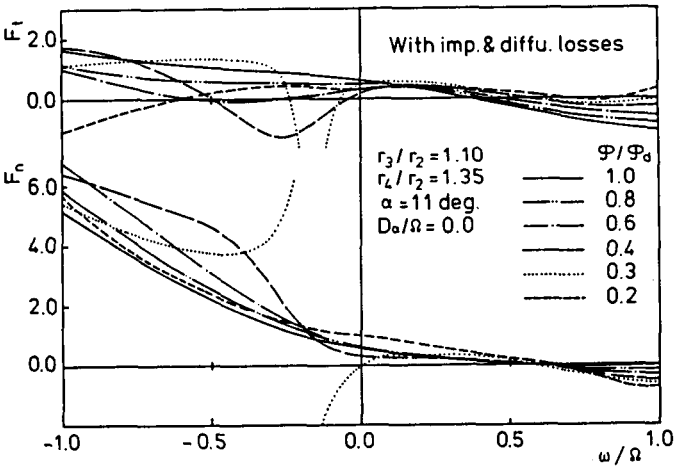

Fig.10 Impeller forces at partial capacities for the case with smaller impeller/diffuser gap. We observe fluctuations of the forces in the range of negative whirl velocity.

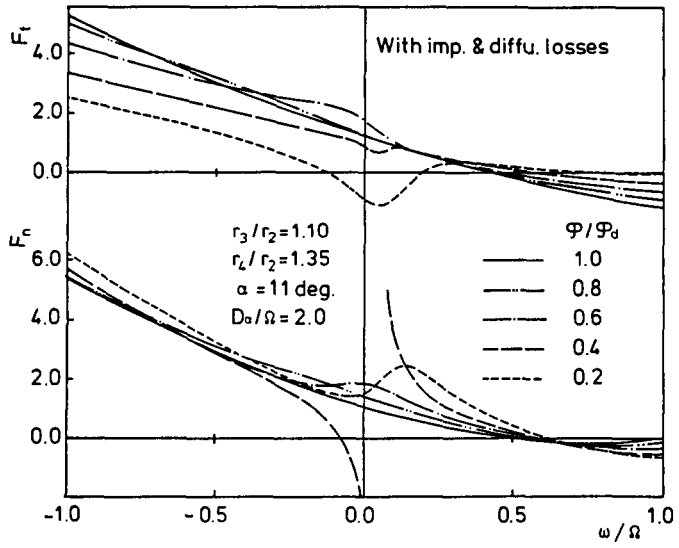

Fig.11 Impeller forces at partial capacities for the case with smaller impeller/diffuser gap. Exponential decay of shed vorticity is considered. Fluctuations in the range of negative whirl velocity diminish and the effects of diffuser rotating stall are observed at small positive whirl velocity.

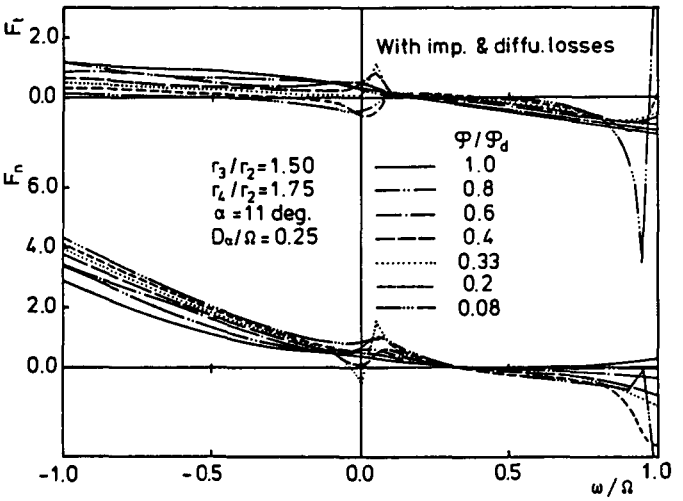

Fig.12 Impeller forces at partial capacities, for the case with larger impeller/diffuser gap. Effects of impeller rotating stall are observed